Plant Science 229 (2014) 53–65

Contents lists available at ScienceDirect

Plant Science

journal homepage: www.elsevier.com/locate/plantsci

# Transcriptional regulation and functional involvement of the Arabidopsis *pescadillo* ortholog *AtPES* in root development

Aris Zografidis[a], Giorgos Kapolas[a], Varvara Podia[a], Despoina Beri[a], Kalliope Papadopoulou[b], Dimitra Milioni[c], Kosmas Haralampidis[a,*]

[a] University of Athens, Faculty of Biology, Department of Botany, 15784 Athens, Greece
[b] University of Thessaly, Department of Biochemistry & Biotechnology, 41221 Larissa, Greece
[c] Agricultural University of Athens, Department of Agricultural Biotechnology, 11855 Athens, Greece

ARTICLE INFO

*Article history:*
Received 19 June 2014
Accepted 21 August 2014
Available online 29 August 2014

*Keywords:*
*Arabidopsis thaliana*
*Pescadillo*
RNAi
Nucleolus
Promoter analysis

ABSTRACT

The Pescadillo gene is highly conserved from yeasts to human and has been shown to impact on both the cell cycle and on ribosome biogenesis. However, the biological function and transcriptional regulation of the plant orthologs remain unclear. In the present study, we have implemented a combination of molecular and genetic approaches, in order to characterize the *Arabidopsis thaliana* pescadillo ortholog (*AtPES*) and its role in root development. The RNAi transgenic lines displayed severely compromised meristem structures and a reduction of the primary root length of up to 70%. The correct pattern of the cell files is distorted, whereas in the root elongation and differentiation zone the epidermal and cortex cells appear abnormally enlarged. Yeast two hybrid and BiFC experiments confirmed that AtPES interacts physically with AtPEIP1 and AtPEIP2, the orthologs of the murine Bop1 and WDR12. Promoter deletion analysis revealed that *AtPES* expression depends on a number of transcription factor binding sites, with the TELO-box being a crucial site for regulating its accurate tissue-specific manifestation. Our results indicate that *AtPES* is firmly regulated at the transcriptional level and that the corresponding protein plays a role in root developmental processes.



## 1. Introduction

The *pescadillo* gene (*pes*) was originally identified and characterized through a mutational screen in zebrafish, affecting embryonic development [1], while Pes1, Nop7/Yph1p and *AtPES* are the murine, yeast and plant orthologs, respectively [2–4]. These conserved nucleolar proteins, which consist of a unique pescadillo N-terminal domain, a phospho-protein binding BRCT domain [5,6] and two motifs for post-translational modification by SUMO-1, appear to participate in a puzzling blend of diverse cellular processes. Overall, pescadillo was shown to be involved in ribosome biogenesis through the processing of pre-rRNAs, cell proliferation control, chromosomal instability, gene regulation and the cytoskeleton [2,6–12].

Ribosome biosynthesis is an enormously complex process conducted in the vicinity of the nucleolus, the specialized organelle for ribosome manufacture [13,14]. In this process, several nucleolar specific protein complexes have been identified and interestingly so, various members of such complexes are not strictly related with the biogenesis of ribosomes, but have been implicated in diverge functions [15]. Such a case is the PeBoW murine complex and the corresponding Nop7–Erb1–Ytm1 complex from budding yeast [16,17]. Pes1 along with the two other members of the heterotrimeric PeBoW complex, namely Bop1 and WDR12, are required for common pre-RNA processing steps and importantly, the integrity of the whole complex has been proved to be indispensable for growth [7,16,18–20]. Research in yeast has come to analogous results. Furthermore, depletion of Nop7/Yph1p leads to a G1 or G2 phase arrest of the cell cycle, providing evidence of a cross-talk between ribosome biogenesis and cell cycle progression [2,8–10,21].

In plants, an implicit prerequisite for the actively dividing cell is the coordination of the cell cycle and growth. A hallmark of the latter is the unperturbed protein synthesis by ribosomes, which in turn highlights the nucleolus as a critical organelle for embryogenesis and development [22]. Advanced level of complexity integrates

* Corresponding author. Tel.:+0030 210 7274131; fax: +0030 210 7274702.
*E-mail addresses:* aristzo@yahoo.gr (A. Zografidis), gkapolas@yahoo.gr (G. Kapolas), vapodia@hotmail.com (V. Podia), debthem@hotmail.com (D. Beri), kalpapad@bio.uth.gr (K. Papadopoulou), bmbi2mid@aua.gr (D. Milioni), kharalamp@biol.uoa.gr (K. Haralampidis).

http://dx.doi.org/10.1016/j.plantsci.2014.08.012
0168-9452/

along the aforementioned demand and novel networks of gene regulation are recruited, so as to assure that active division takes place in specific places and in an overall controlled way for the whole organism [23–27]. In Arabidopsis, a number of embryo lethal mutants and the responsible genes (e.g. *MEE49*, *SLOW WALKER2*, *TAN* and *At-eIF6*) have been characterized and found to correspond to *Saccharomyces cerevisiae* orthologs nucleolar proteins, all of which co-immunoprecipitate with Nop7/Yph1p (Supplementary Table A.2).

More recent data by Cho et al. [28], also show that pescadillo plays an essential role in plant growth and survival. Gene silencing of plant *PES* leads to growth arrest and acute cell death. Like Pes1, plant PES was also found to play a role in chromosome segregation. However, while Pes1 is associated with the periphery of metaphase chromosomes, plant PES is distributed along spindles and phragmoplasts during mitosis, indicating that their molecular mechanisms and protein interactions are likely to be different. Furthermore, the authors suggest that plant PES may have dual function in interphase and mitosis, possibly through interactions with different partners [7,10,16,28].

We have previously shown that *AtPES* encodes the *Arabidopsis thaliana* ortholog of Nop7 and that the two proteins exhibit a functional conservation [4]. In this study, we have determined the protein interaction partners of AtPES and have further investigated its role in root development. Moreover, the transcriptional regulation of *AtPES* was studied using promoter deletion analysis and site directed mutagenesis approaches.

## 2. Materials and methods

### 2.1. Plant material and growth conditions

*A. thaliana* (L.) Heynh. (ecotype Columbia) were used in this study. T-DNA insertion mutants were obtained from the ABRC *Arabidopsis* stock center. Wild-type and transgenic *Arabidopsis* plants and *Nicotiana benthamiana* plants were grown under standard conditions at 22 °C in 70% humidity with a light/dark cycle of 16 h/8 h and illumination of 110 $\mu E\,m^{-2}\,s^{-1}$ PAR supplied by cool-white fluorescent tungsten tubes (Osram, Germany). Seeds from individual T2 or T3 transgenic *Arabidopsis* plants were germinated under sterile conditions on selective half strength Murashige and Skoog medium containing 20 mg $L^{-1}$ hygromycin or 40 mg $L^{-1}$ kanamycin and 200 mg $L^{-1}$ cefotaxime. Ten to twelve transgenic plants were transferred to soil for further development and analysis. For estradiol treatments, transgenic and control plants were germinated and grown for 7, 10 or 14 days in MS medium containing 30 μM 17-β-estradiol dissolved in DMSO. For the RT-PCR analysis showing the accumulation of unprocessed 32S pre-RNAs, plants were germinated and grown for 10 days in MS medium containing 30 μM 17-β-estradiol dissolved in DMSO, or in MS medium containing only DMSO as a control.

### 2.2. RNA extraction, cDNA synthesis and semiquantitative RT-PCR analysis

Total RNA was extracted from *A. thaliana* samples with the RNeasy Plant Mini Kit (Qiagen) according to the manufacturer's instructions. First strand cDNA was synthesized from two micrograms of total RNA in a volume of 20 μL with Expand Reverse Transcriptase (Roche) according to the manufacturer's protocol. PCR amplifications were performed with primers specific for targeted genes (Supplementary Table A.1) and according to the needs of plasmid construction. The PCR products were separated by electrophoresis on 1% agarose gels and visualized by ethidium bromide staining (100 μg $L^{-1}$).

### 2.3. Construction of RNAi and overexpression vectors

For generating the *AtPES* interference construct, the first 530 bp of the *AtPES* ORF was amplified by PCR using primer pair PESiXhoI and PESiKpnI, and cloned into the XhoI/KpnI linearized pHANNIBAL vector, generating construct pHANNIBAL::PESa. The same fragment of *AtPES* was PCR amplified using primer pair PESiClaI and PESiBamHI, and cloned into the ClaI/BamHI sites of pHANNIBAL::PESa, generating vector pHANNIBAL::PESi. The SpeI/XhoI fragment of pHANNIBAL::PESi, harboring the hairpin construct [$_{\rightarrow}$AtPES$_{530}$–intron–AtPES$_{530\leftarrow}$] was subsequently cut out and ligated into the respective sites of the estrogen-inducible pER8 vector [29], generating vector pER8::PESi.

For generating transgenic *Arabidopsis* lines overexpressing *AtPES*, the entire *AtPES* cDNA was amplified by PCR using primers oAtPESF (with an added BamHI site) and oAtPESR (with an added SacI site). The product was then digested and ligated into the BamHI/SacI linearized pBI121 (Clontech) binary vector, downstream of the CaMV 35S promoter, generating construct pB35PES. High fidelity DNA polymerases (Roche, New England Biolabs) were used for all amplifications and the constructs were confirmed by sequencing or restriction enzyme analysis.

### 2.4. Protein interaction in yeast two-hybrid assays

The first-strand cDNA, synthesized as described above, was used to amplify by PCR *AtPES*, *AtPEIP1* and *AtPEIP2* ORFs with primer pairs 2hNdeI5pes/2hBamHI3pes, 2hSmaI5P1/2hBamHI3P1 and 2hEcoRI5P2/2hSalI3P2, respectively. The Expand™ High Fidelity PCR System (ROCH) was used for all PCR reactions, according to the manufacturer's protocol. The respective amplified products were cloned into the pGADT7 and pGBKT7 yeast two hybrid vectors (Clontech) as follows: *AtPES* (At5g14520) was cloned as an NdeI–BamHI fragment to both pGADT7 and pGBKT7 generating pGADT7::*AtPES* and pGBKT7::*AtPES* constructs, respectively; *AtPEIP1* (At2g40360) was cloned as an XmaI–BamHI fragment to pGADT7 generating plasmid pGADT7::*AtPEIP1*; *AtPEIP2* was cloned as an EcoRI–SalI fragment to both pGBKT7 and pGADT7 (using EcoRI–XhoI restriction sites of pGADT7) generating plasmids pGBKT7::*AtPEIP2* and pGADT7::*AtPEIP2*, respectively. The aforementioned vector constructs were used for the transformation of yeast strain Y187 (*MATα*, *ura3-52*, *his3-200*, *ade2-101*, *trp1-901*, *leu2-3, 112*, *gal4Δ*, *met-*, *gal80Δ*, *MEL1*, *URA3*::*GAL1UAS-GAL1TATA-lacZ)*, according to the standard lithium acetate protocol (Clontech). Double transformed yeast colonies were selected on a synthetic dropout medium without Trp and Leu (SD, trp-, leu-) and restreaked on SD/-Trp/-Leu medium containing 1% raffinose, 2% galactose and 80 mg $L^{-1}$ X-α-Gal. Yeast growth and galactosidase activity was analyzed after 3–4 d at 30 °C.

### 2.5. Bimolecular fluorescence complementation (BiFC)

*A. thaliana* cDNA, synthesized as described above, was used to amplify by PCR *AtPES*, *AtPEIP1* and *AtPEIP2* ORFs with the primer pairs SpAtPESF and SpAtPESR, SpPEIP1F and SpPEIP1R, and SpPEIP2F and SpPEIP2R, respectively. The PCR products were blunt-end ligated into the SmaI-linearized pUC18 cloning vector, generating plasmids pUC18::*AtPES*, pUC18::*AtPEIP1* and pUC18::*AtPEIP2*. *AtPES* was subsequently subcloned as an KpnI–XmaI fragment into the pSPYNE-35S BiFC vector, generating plasmid pSPYNE-35S::*AtPES*. *AtPES* was also subcloned as an BamHI–XmaI fragment, derived from pSPYNE-35S::AtPES, into pSPYCE-35S, generating plasmid pSPYCE-35S::AtPES. *AtPEIP1* and *AtPEIP2* were subcloned as BamHI–XmaI and SalI–XmaI fragments into the pSPYCE-35S and pSPYNE-35S BiFC vector, generating plasmids pSPYCE-35S::*AtPEIP1*, pSPYCE-35S::*AtPEIP2*,

pSPYNE-35S::*AtPEIP1* and pSPYNE-35S::*AtPEIP2*, respectively. All constructs were transferred into *A. tumefaciens* GV3101 competent cells via the general freeze–thaw method [30] and the transformed bacteria were used for the transient transformation of epidermal cells of *N. benthamiana* leaves. Experiments were carried out using all possible combinations of agrobacteria harboring the pSPYNE and pSPYCE constructs, alongside with all respective negative controls (e.g. pSPYNE-35S::AtPES + pSPYCE-35S) and the positive control pSPYNE-35S::bZIP + pSPYCE-35S::bZIP [31].

### 2.6. In silico promoter analysis

The 454 bp promoter sequence of *AtPES* (locus At5g14520), designated herein as *AtPES*p, was retrieved from TAIR (The Arabidopsis Information Resource, http://www.arabidopsis.org/). For the retrieval of other promoters of plant *pescadillo* orthologs, an AtPES protein tblastn query was initially conducted on non-annotated data (whole genome shotgun sequencing, GenBank) available for *Vitis vinifera*, *Glycine max*, *Populus trichocarpa*, *Oryza sativa*, and *Sorghum bicolor*. Sequence information of approximately 700 bp upstream of the first AUG codon from the aforementioned angiosperm *pescadillo* orthologs, designated, respectively, as VvPESp, GmPESp, PtPESp, OsPESp and SbPESp, were subsequently retrieved for analysis. All promoters were analyzed *in silico* using PLACE software (http://www.dna.affrc.go.jp/PLACE/) and NSITEM-PL software available at Softberry (http://linux1.softberry.com/berry.phtml). AtPESp was also analyzed using AtCOECiS (http://bioinformatics.psb.ugent.be/ATCOECIS/).

### 2.7. AtPES promoter deletion analysis

*A. thaliana* genomic DNA was isolated from leaf tissue ground in liquid nitrogen via standard procedures (SDS extraction/phenol–chloroform purification). The genomic DNA was subsequently used to amplify by PCR *AtPES* promoter fragments of 122 bp, 172 bp, 192 bp, 256 bp and 572 bp upstream of the translation initiation codon, using primer pairs PESpdaR1/PESpdaF1, PESpdaR1/PES-S2F1, PESpdaR1/PES-S2F2, PESpdaR1/PESpdaF2 and PESpdaR1/PESpdaF3, respectively. The Expand™ High Fidelity PCR System (ROCHE) was used for all PCR reactions according to the manufacturer's protocol. PCR products of 122 bp, 256 bp, and 572 bp were initially cloned as SalI–PstI fragments into the respective sites of pUC19 and then subcloned ahead of the *b*-glucuronidase (GUS) gene as SalI–HindIII fragments into the PGTV-HPT binary vector, generating plasmids PGTV-HPT::pAtPES122, PGTV-HPT::pAtPES256 και PGTV-HPT::pAtPES572, respectively. PCR products of 172 bp and 192 bp were directly cloned as SalI–HindIII fragments into vector PGTV-HPT, generating plasmids PGTV-HPT::pAtPES172 and PGTV-HPT::pAtPES192, respectively. For the conversion of the TELO-box cis-element A**AA**CC**C**TAA to the mutagenized muTELO-box A**TT**CC**G**TAA, a PCR based site-directed mutagenesis procedure was conducted, using pUC19::pAtPES192 and pUC19::pAtPES256 as DNA templates and the primer pair muTELO1/muTELO2. The mutagenized fragments p*AtPES*muTELO192 και p*AtPES*muTELO256 were then subcloned into the linearized SalI–HindIII PGTV-HPT vector, generating plasmids PGTV-HPT::pAtPESmuTELO192 and PGTV-HPT::pAtPESmuTELO256, respectively.

Histochemical staining for GUS activity was performed on T2 and T3 transgenic plants using 5-bromo-4-chloro-3-indolyl-β- D-glucuronide (X-Gluc) as a substrate. Tissues were stained for 2 h at 37 °C in X-Gluc reaction buffer (50 mM sodium phosphate buffer, pH 7.2, 0.5 mM potassium ferrocyanide, 0.5 mM potassium ferricyanide, and 2 mM X-Gluc), dehydrated by a series of ethanol washes, and kept in 3.7% (w/v) formaldehyde, 50% (w/v) ethanol, and 5% (w/v) acetic acid at 4 °C. Quantitative analysis of GUS activity was measured by monitoring cleavage of the β-glucuronidase substrate 4-methylumbelliferyl β-D-glucuronide (MUG), using a LS50B Perking Elmer luminescence spectrometer.

### 2.8. Plant transformation

*A. tumefaciens* strain GV3101 competent cells were transformed with the aforementioned constructed vectors by using the general freeze–thaw protocol [30] and the transformed bacteria were subsequently used for the stable transformation of *A. thaliana* plants via the vacuum infiltration method as previously described [31].

Agrobacterium-mediated transient transformation of tobacco leaf tissues was carried out as described previously [32,33] with minor modifications. Agrobacterium strains (GV3101), harboring the BiFC constructs, were co-infiltrated into the abaxial air space of 4–6-week-old plants, alongside with a strain carrying the p19 Suppressor from tomato bushy stunt virus (TBSV). Co-infiltration of strains containing the BiFC constructs and the p19 silencing plasmid was carried out at $OD_{600}$ of 0.8:0.8:1.0. Epidermal cell layers of tobacco leaves were assayed for fluorescence 2–3 days after infiltration.

### 2.9. Microscopy

Root meristem organization and nuclei were visualized using WT and T3 transgenic RNAi or overexpressor lines stained with Hoechst dye. Seedlings were fixed in 4% (wt/vol) PFA in PEM (50 mM Pipes, 5 mM EGTA, 5 mM $MgSO_4$, pH 6.9, with KOH) for 15 min, followed by washing for 5 min in PEM buffer. Fixed seedlings were washed with phosphate buffered saline (PBS), stained with 10 $\mu g\,mL^{-1}$ Hoechst 33258, and then washed with PBS buffer three times. Samples were examined with an Axioscope fluorescence microscope and photographed with an Axiocan MRc digital camera (Zeiss, Germany).

For the BiFC experiments, 48–72 h upon transformation, tissue samples of leaf epidermis were prepared in a drop of water and were subsequently examined and photographed with an epi-illumination fluorescence microscope (Zeiss, Germany), using a filter set consisting of a blue filter (excitation, 450–490 nm; dichroic mirror, 510 nm; barrier filter, 520 nm), a green barrier filter (515–565 nm) and a red long pass filter (647 nm).

Histochemical GUS staining of transgenic plants were performed as described above. Samples were observed and photographed using a stereomicroscope (Zeiss, Stemi 2000-C) or a differential interference contrast microscope (Olympus, BX50). All images were processed by using Adobe Photoshop CS5 Extended software.

## 3. Results

### 3.1. Root phenotype of the induced AtPES RNAi lines

To elucidate the function of AtPES in plant development, several independent lines carrying putative T-DNA insertions in gene locus At5g14520 were obtained from the Arabidopsis Biological Resource Center (ABRC). Since the insertion could not be verified by PCR in any of the SALK lines, a post-transcriptional silencing approach mediated by RNA interference (RNAi) was carried out. To downregulate *AtPES*, we generated an RNAi construct (pER8::*PESi*), harboring a 530 bp inverted repeat of the *AtPES* ORF and placed it under the control of an estrogen-inducible promoter (Fig. 1A). The analysis of ten independent transgenic lines showed that downregulation of *AtPES* expression, resulted in a series of interesting root phenotypes. Overall, a reduction in the length of the primary root, ranging from 10% to 70%, was observed in 8 out of the 10

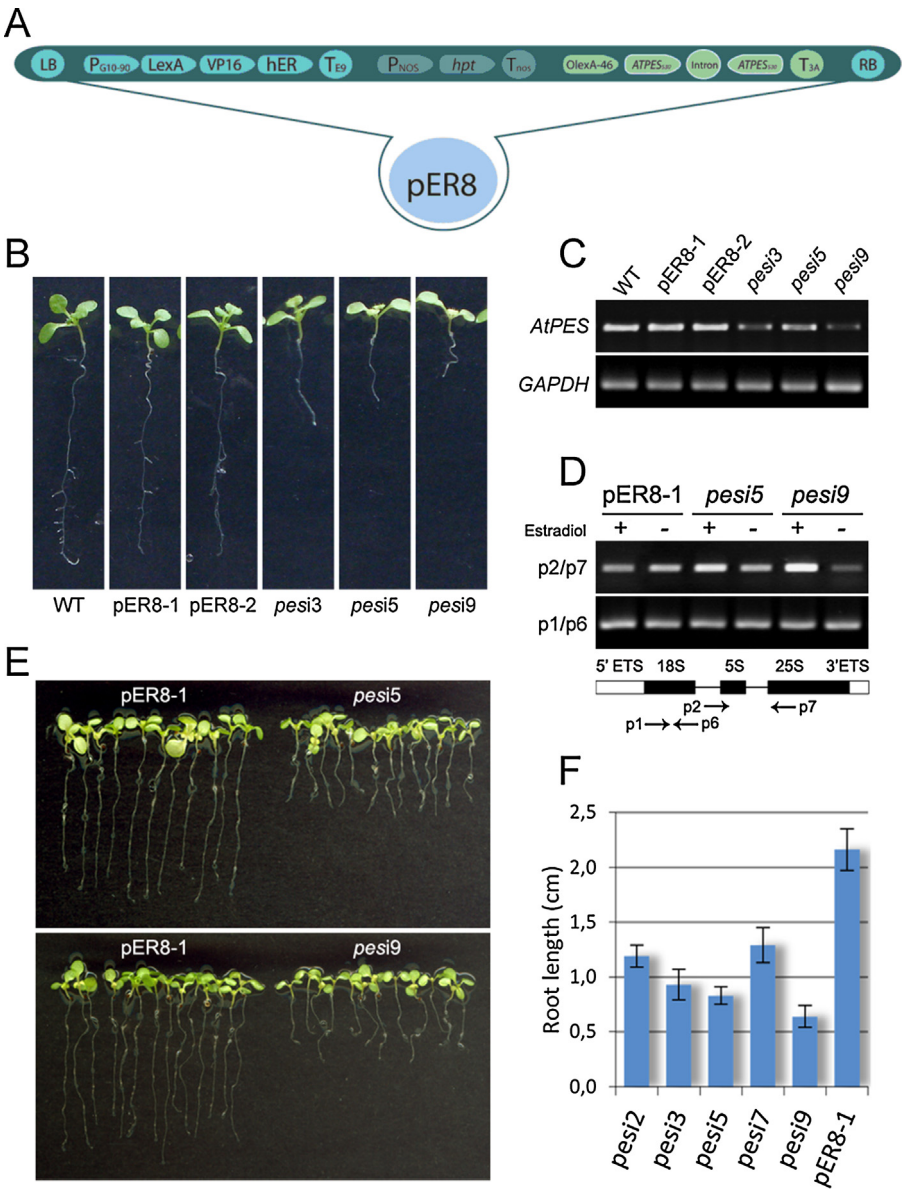


**Fig. 1.** Analysis of *AtPES*–RNA interference lines. (A) Schematic representation of the estrogen-inducible pER8::*PESi* hairpin construct [→AtPES$_{530}$–intron–AtPES$_{530}$←]. (B) Representative plant phenotypes of WT, two control lines (pER8-1 and pER8-2) and three *AtPES*–RNA interference lines (*pesi*3, *pesi*5 and *pesi*9) grown on MS medium supplemented with β-estradiol. (C) RT-PCR of *AtPES* specific mRNA transcripts in root tissues of WT, pER8 and three *pesi* transgenic lines. (D) Detection of 32S pre-rRNA in root tissues of a control (pER8-1) and two RNAi lines (*pesi*5 and *pesi*9) grown on MS medium supplemented with β-estradiol or DMSO alone as a control. Bottom diagram shows the Arabidopsis pre-rRNA transcript and the primers used to detect the 18S and 32S pre-rRNAs by RT-PCR. (E) Micrograph showing on the right seedlings of *AtPES*–RNAi lines (*pesi*5 and *pesi*9) and on the left seedling of the control pER8-1 line grown on MS medium supplemented with β-estradiol. Note the significant reduction in root length of the RNAi lines compared to the control. (F) Statistical evaluation of root length for 10 days-old RNAi (lines *pesi*2, *pesi*3, *pesi*5 *pesi*7 and *pesi*9) and control plants grown on MS medium containing β-estradiol.

independent lines (Fig. 1B, E and F). RT-PCR analysis revealed that the silenced plants had reduced *AtPES* mRNA levels and accumulated unprocessed 32S pre-RNAs, compared to those transformed with the empty pER8 vector, signifying that the observed phenotypes were indeed related to the disrupted AtPES activity, after the induction by 17β-estradiol (Fig. 1C and D).

A closer microscopic examination revealed that the affected lines had a variety of severely compromised root structures, displaying a series of phenotypic anomalies (Figs. 2 and 3). The roots are characterized by a significant shortening of the meristematic and elongation zone. While the meristem size of the control pER8 roots is about 300 μm long, *pesi-5* and *pesi-9* roots display a meristem size no longer than 100 μm. The corresponding meristem cell number is also significantly reduces. The meristem of the control pER8 roots consist of about 34 cells per file, while no more than 12 cells were counted in the *pesi* lines, which is in accordance to the reduced number of cells observed to contain mitotic nuclei (Fig. 3A–D and J). Furthermore, these cells appear abnormally enlarged compared to wild-type (WT) and control pER8 root meristem cells, which have nearly constant sizes (Fig. 3G and H). In the differentiation zone, as indicated by the concurrent appearance of xylem vessels in the vasculature at that point, the cells display a deformed and bulged phenotype (Figs. 2 and 3C and D).

Previous reports have shown that root meristem cells of WT seedlings remain within the mitotic cell cycle and have nuclei with nearly constant sizes. Further up, in the differentiation zone of the root, nuclei undergo endoreduplication cycles, which

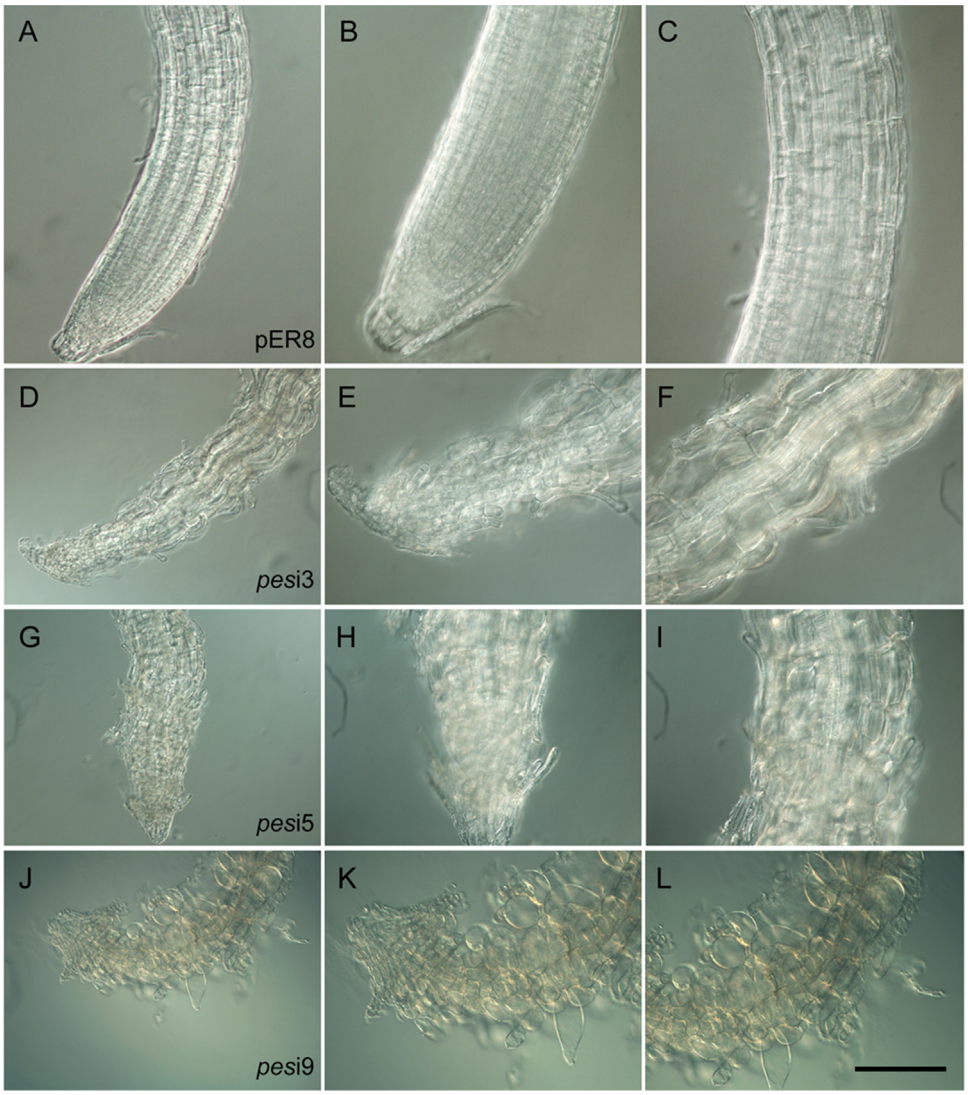


**Fig. 2.** Root phenotypes of *AtPES*–RNAi lines. Transgenic plants were grown for 10 days in inductive MS medium containing β-estradiol before being photographed. B and C, magnification of the root meristematic and elongation zone of the pER8-1 control plant (A). (E), (F), (H), (I), (K) and (L), magnification of the meristematic and elongation zone of RNAi line *pesi*3 (D), *pesi*5 (G) and *pesi*9 (J), respectively. Aberrant cell division planes and abnormal expansion of cells were observed in all layers. Bar = 100 μm for left column and 70 μm for middle and right column.

concomitantly lead to an increase of their size [34]. Fluorescence microscopy of Hoechst-stained nuclei revealed that 10-d-old WT root tips contain a large number of meristematic cells with mitotic nuclei (Fig. 3B and G). In the *AtPESi* lines, however, this cell population is mostly replaced by cells containing much larger nuclei, which are comparable with those found in more mature WT cells of the elongation and differentiation zone (Fig. 3H–J). The above results indicating that the disruption of *AtPES* function affects normal root cell growth and differentiation in Arabidopsis.

### 3.2. Analysis of transgenic A. thaliana plants overexpressing AtPES

The function of *AtPES* in plant development was further investigated in *AtPES* overexpression lines (oLs). The *AtPES* coding region was placed under the control of the CaMV 35S promoter and introduced into Col-0 wild-type plants (Fig. 4A). Overexpression of *AtPES* was determined in 9 transgenic lines (oL1-9) by semi-quantitative RT-PCR. As shown in Fig. 4B, the expression level of *AtPES* varied between different transgenic lines, ranging at least 4- to 8-fold higher than in WT plants. However, all overexpressing lines exhibited a wild-type root and shoot phenotype throughout development and no morphologically abnormal growth phenotypes were observed (Fig. 4C and D). The length of the primary root as well as the number of lateral roots per plant in the overexpressing lines was statistically similar to that of WT plants (Fig. 4E). Flower morphology, fertility and seed set were also similar in both oL and WT plants (data not shown). The above results indicating that overexpression of *AtPES* does not influence or alter the normal developmental program of Arabidopsis.

### 3.3. Protein interactions of AtPES

The AtPES-GFP fusion protein is localized predominantly in the nucleolus of the root epidermal cells [4]. Based on the plant nucleolar architecture, as seen by conventional electron microscopy [35,36] and in agreement with its putative function, AtPES localization appears to coincide with the granular component of the plant nucleolus, the site of internal spacer 1 excision and pre-ribosomal subunit assembly (Supplementary Fig. A.1).

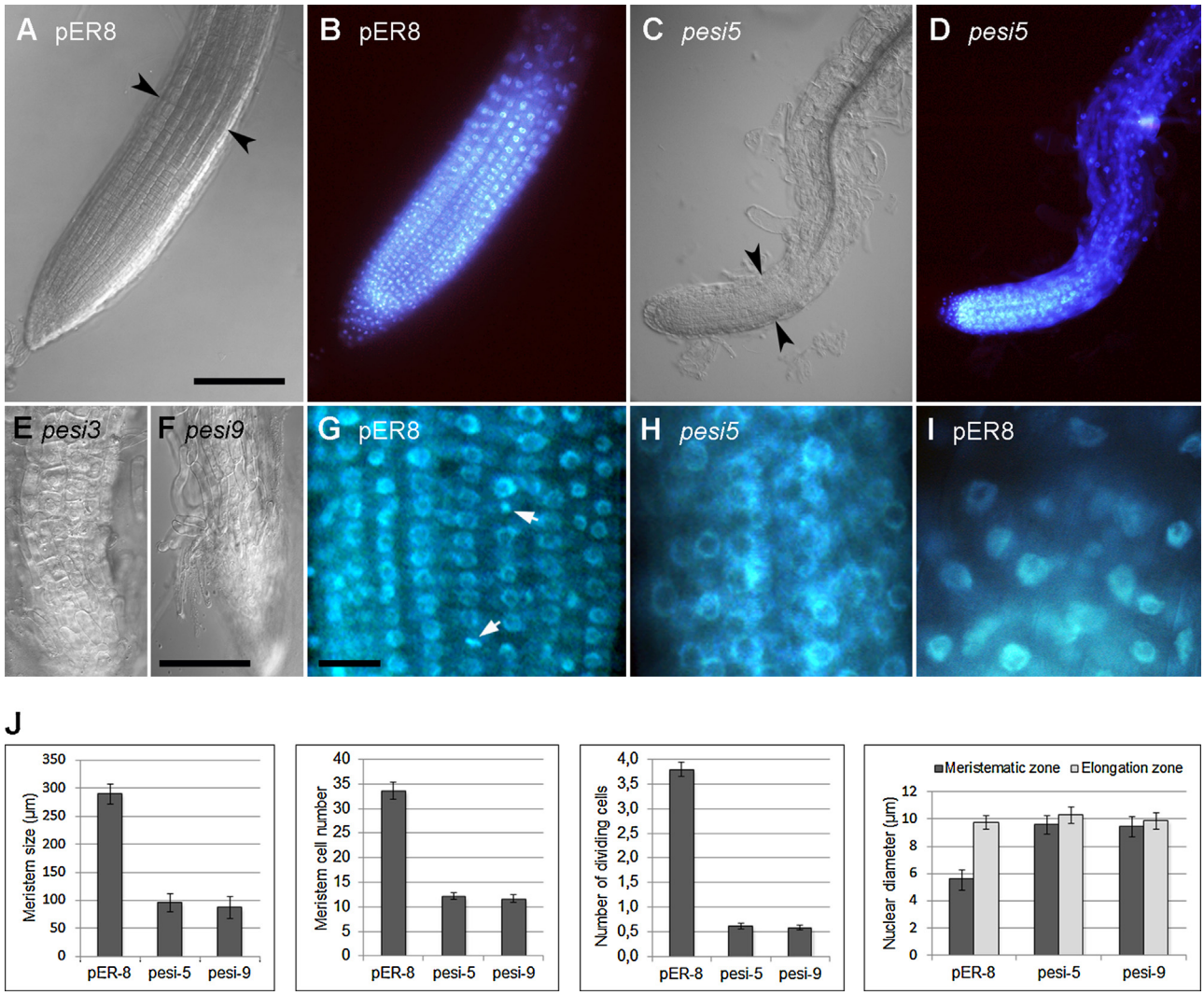


**Fig. 3.** Silencing of *AtPES* severely disrupts normal root development. Fluorescence and DIC (Nomarski) microscopic images from pER8 control and *AtPES*–RNAi lines stained with Hoechst. Root samples were viewed and photographed, after 10 days ((A)–(D) and (G)–(I)) or after 14 days ((E) and (F)) in inductive MS medium containing β-estradiol, under epifluorescence optics with blue excitation ((B), D–(G)) or under DIC optics ((A) and (C)). Black arrows indicate the approximate position of the boundary between meristematic and elongation zone. White arrows show mitotic nuclei with condensed chromosomes. Bar = 100 μm for (A) to (D), 50 μm for (E) and (F) and 20 μm for (G) to (I). (J) Root meristem size, meristem cell number (cortex), number of dividing cells and nuclear diameter of meristematic and elongation zone cells in pER8 control and *AtPES*–RNAi lines (*pes*i5 and *pes*i9) after 10 days in inductive MS medium containing β-estradiol. Results are presented as means ± SE from three experiments ($n = 20$). (For interpretation of the references to color in this figure legend, the reader is referred to the web version of this article.)

In view of the existence in both animals and yeast of a *pescadillo* involving heterotrimeric complex, specifically the PeBoW murine complex and the corresponding Nop7–Erb1–Ytm1 complex from budding yeast, we examined whether such a protein complex is also conserved in plants. By scanning the *A. thaliana* Nucleolar Protein Database (AtNoPDB), we were able to identify the Arabidopsis Bop1/Erb1 ortholog (At2g40360) and WDR12/Ytm1 ortholog (At5g15550), designated hereafter as AtPEIP1 and AtPEIP2, respectively. AtPEIP1 and AtPEIP2 display an amino acid similarity to Erb1 and Ytm1 of 57% and 48%, respectively (Supplementary Table A.4). Bop1 and WDR12, their yeast counterparts Erb1 and Ytm1 as well as AtPEIP1 and AtPEIP2 are all WD40 repeat domain-containing proteins. The WD40 repeat is an ancient sequence motif that has been identified in a diverse group of functionally distinct proteins involved in miscellaneous cellular processes, including gene transcription, signal transduction, and mRNA modification [37]. While both *AtPEIP1* and *AtPEIP2* are as yet uncharacterized, transcriptional profiling and experimental data show that they encode nucleolar proteins [4,28]. In order to investigate the potential physical interactions between AtPES, AtPEIP1 and AtPEIP2, we employed two independent methods.

As shown in Fig. 6, AtPES interacted physically with either AtPEIP1 or AtPEIP2 in yeast two-hybrid assays, providing evidence for the existence of a corresponding complex in Arabidopsis (Fig. 5B). The interactions were also confirmed *in planta*, by bimolecular fluorescence complementation (BiFC) assays in *N. benthamiana* (Fig. 5A). The co-transformation of tobacco epidermal cells, with plasmids harboring the *AtPES* and *AtPEIP1* or *AtPES* and *AtPEIP2* BiFC constructs, resulted in a clear fluorescent signal localized in the nucleolus of the cells (Fig. 5A). We were unable to obtain a positive interaction signal with either of the methods, when AtPEIP1 and AtPEIP2 were used as interacting partners. However, by using BiFC and Co-IP in tobacco protoplasts, Cho et al., were able to confirm that AtPEIP1 (BOP1) and AtPEIP2 (WDR12) interact also with each other, indicating that the heterotrimeric complex is also conserved in plants [28]. Our failure to confirm the direct interaction of AtPEIP1 and AtPEIP2 could be either due to the different methodology and/or tissue used.

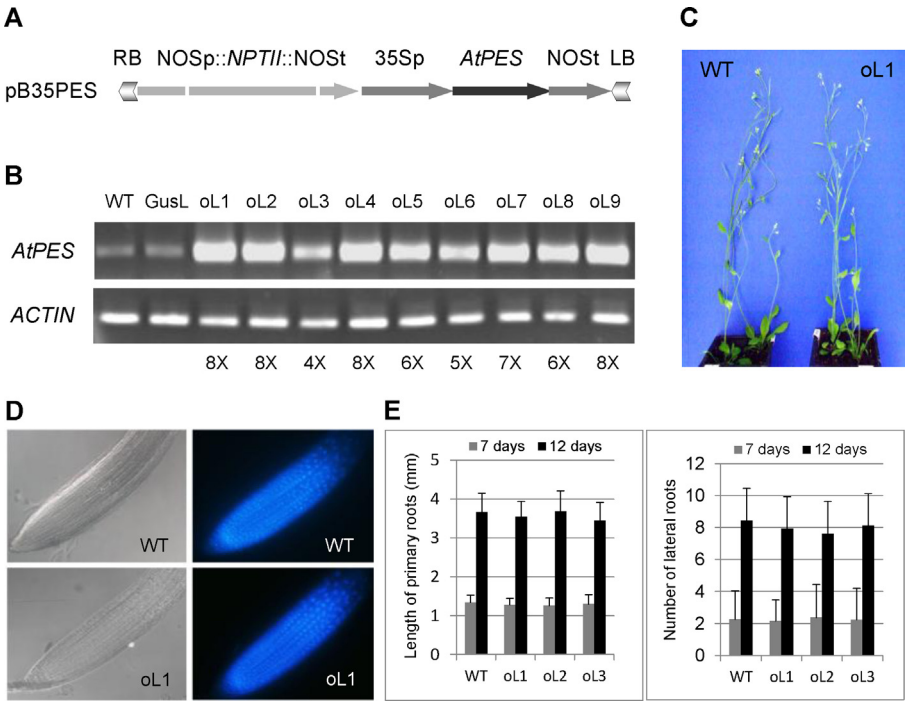


**Fig. 4.** Analysis of *A. thaliana* plants overexpressing *AtPES*. (A) Schematic representation of the T-DNA region of the binary vector (pB35PES) used to generate *Arabidopsis* plants overexpressing *AtPES*. RB and LB, right and left border, respectively; NOSp, nopaline synthase gene promoter; *NPTII*, neomycin phosphotransferase gene; NOSt, nopaline synthase terminator; 35Sp, CaMV 35S gene promoter; *AtPES*, entire coding region of *AtPES* cDNA. (B) RT-PCR gel blots showing the transcript levels of *AtPES* and *ACTIN* in WT plants, one GUS reporter line (GusL) and 9 overexpressors (oL1–oL9). Numbers at the bottom indicate times-fold increase of *AtPES* transcripts in oLs compared to WT. (C) Phenotypes of mature (36 days) WT and oL1 overexpressor plants. (D) Fluorescence and DIC (Nomarski) microscopic images from WT and oL1 line, stained with Hoechst. Root samples were viewed and photographed after 10 days under epifluorescence or DIC optics. (E) Length of primary roots and number of lateral roots per plant, as measured in WT plants and three overexpressor lines (oL1, oL2 and oL3), after 7 and 12 days in MS medium. Results are presented as means ± SE from three experiments ($n = 20$).

### 3.4. Identification of putative regulatory elements within the AtPES promoter

*AtPES* is mainly expressed in the actively dividing cells of the vegetative and reproductive tissues. GUS staining is evident in the shoot and root apical meristems, the leaf primordial and the developing and mature pollen ([4] and present study). In an attempt to gain insight into the particular regulatory networks that guide this expression, we conducted an in depth *in silico* analysis of the *AtPES* promoter sequence.

In addition to the predicted TATA-box (TATAT), which is located at position −115, the analysis revealed the existence of several other putative *cis* regulatory elements. A canonical TELO-box (AAACCCTAA) is found at position −69 alongside with one direct and two inverted site-II motifs (AGCCCA/C) at positions −180, −169 and −122, respectively (Fig. 6A). The TELO-box, representing the binding site of *At*Purα, has been found in the promoters of numerous genes expressed in cycling cells and Arabidopsis genes encoding ribosomal proteins. Its conserved topological association with either the *tef*-box (ARGGRYANNNNNGTM) or the site-II motifs (the binding sites of *At*TCP-20) regulates gene expression in secondary root meristem primordial [38–40]. A bioinformatics analysis revealed that apart from the *AtPES* promoter, TELO-boxes and site-II motifs are also harbored within the promoters of other angiosperm *AtPES* orthologs, which moreover exhibit an apparent topological homogeneity. The conserved orientated TELO-box resides between 69 and 89 bp upstream of the ATG, while the first site-II motif is found 44 to 79 bp upstream of the TELO-box (Supplementary Table A.3).

Furthermore, the *AtPES* promoter contains an inverted CCAAT-box (enhancer of transcription element) at position -182, partially overlapping the first site-II motif, and a R2R3 MYB4 transcription factor binding site (AACAAAC) at position −202. A CArG-box (CCTTAAAAGC), [41], demonstrated to bind MADS-domain containing proteins at the core consensus binding site $CC(A/T)_6(G/C)_2$, is also present at position −176 (Fig. 6A). In plants, the CArG-box has been shown to be a binding site for the common wheat MADS-box protein VRT2 [42] and to regulate transcription of the Arabidopsis floral homeotic gene *APETALA3* [43,44].

### 3.5. Assessment of putative TFBS by GUS-assisted expression analysis

In order to evaluate the contribution of the identified regulatory *cis*-acting elements in *AtPES* expression during plant growth and development, we generated a series of transgenic Arabidopsis lines designed to express the β-glucuronidase (GUS) gene under the control of various, successive deletions of the *AtPES* promoter. GUS activity, which was monitored in at least eight independent transgenic lines for each construct both qualitatively and quantitatively, revealed that the *AtPES* promoter contains both negative and positive regulatory elements.

Plant lines harboring the full-length promoter transgene (construct pA454), showed a similar GUS expression pattern to that observed previously in transgenic lines harboring an independently generated promoter construct [4]. In seedlings, deletion of the promoter to point −265 (construct pA265) resulted in a slight increase in GUS activity. However, further deletion of the promoter to point −190 (construct pA190) showed a 7-fold increase in GUS activity, when compared to the full length promoter, indicating that negative *cis*-regulatory elements are present in the region within positions −454 to −265 and especially in the region within positions −265 to −190 (Fig. 8A). In agreement to the quantitative measurements, GUS staining in transgenic plants harboring constructs pA454 or pA265 is restricted predominantly in the meristematic zones and the developing root and shoot primordial.

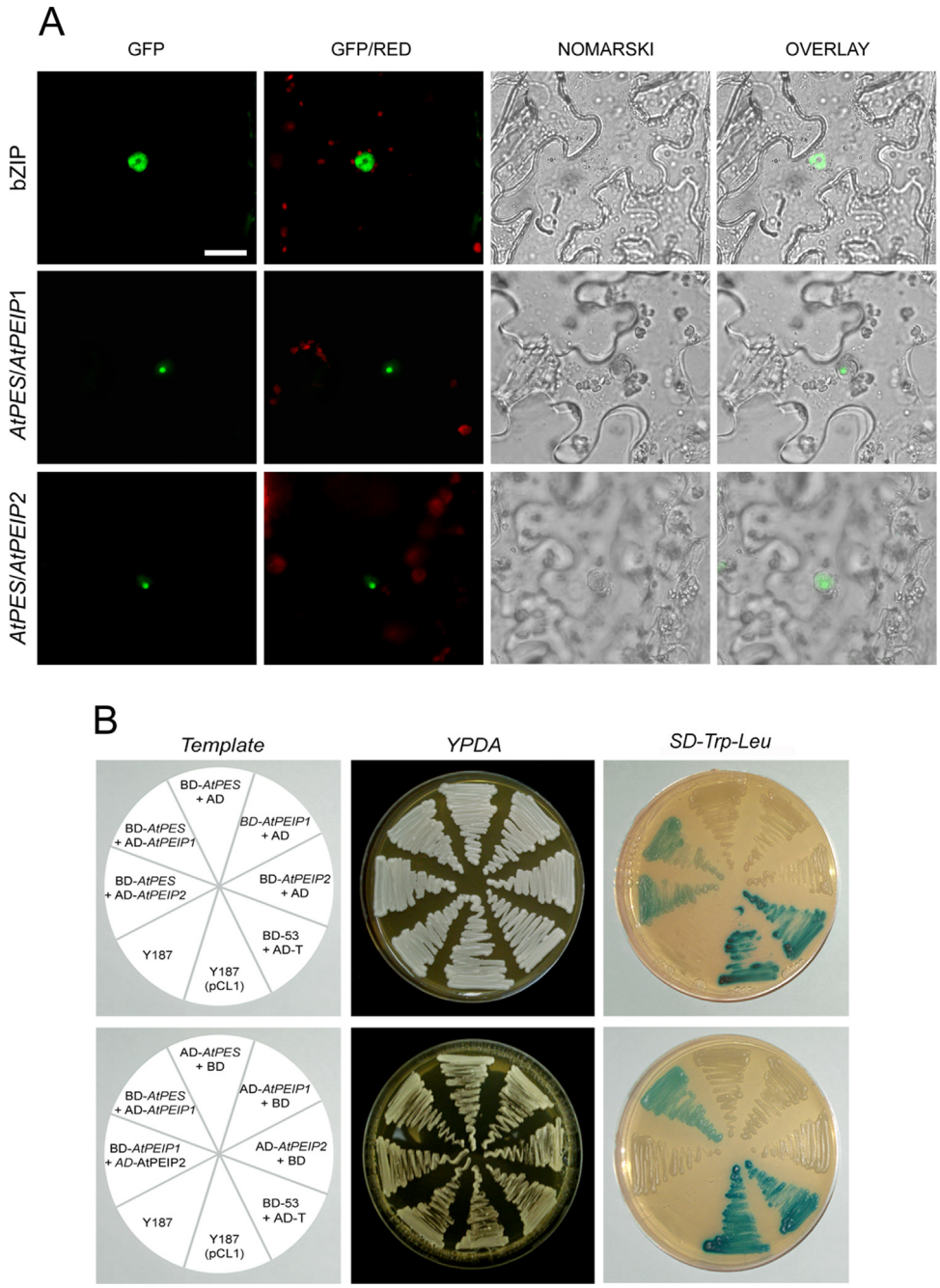


**Fig. 5.** Visualization of protein–protein interactions using BiFC in living cells and two-hybrid analysis in yeast. (A) Fluorescence and DIC (Nomarski) images of *N. benthamiana* epidermal cells expressing the proteins indicated in each lane were acquired 36–48 h after transformation. BiFC fluorescence is indicated by the GFP signal. Individual and merged epifluorescence images of GFP and autofluorescence of chlorophyll as well as DIC images of tobacco epidermal cells are shown. Middle and bottom lanes show protein interactions among *AtPES1* and *AtPEIP1* or *AtPES1* and *AtPEIP2*, respectively. As a positive control epidermal cells were transformed with the pSPYNE-35S and pSPYCE-35S vectors harboring the bZIP63 sequence (upper lane). Scale bar = 25 μm. (B) Heterodimerization of *AtPES1* and *AtPEIP1* or *AtPEIP2* in yeast. The first panel shows the template of the indicated Gal4 DNA-binding domain (BD) and activation domain (AD) constructs used to transform yeast strain Y187. Co-transformants were selected and assayed for the activity of protein–protein interaction on a synthetic dropout medium (SD-Trp-Leu) containing X-α-Gal. Streaked out positive control (BD-53/AD-T and pCL1) and negative control colonies (BD-*AtPES1*/pGADT7, BD-*AtPEIP1*/pGADT7 and BD-*AtPEIP2*/pGADT7) are also shown.

Apart from the minor increase in GUS activity, the tissue specific expression pattern is not altered (Fig. 7A–C). Construct pA190, however, shows a strong overall GUS staining pattern, which extended into almost all tissues of the seedling (Fig. 7F–H). Interestingly, the region within positions −265 to −190 contains a R2R3 MYB4 binding site, which has previously been shown to bind a novel group of plant R2R3 MYB proteins involved in transcriptional silencing [45,46]. Most intriguing, further deletion of the promoter up to point −172 results in a complete abolishment of gene expression, even though the fragment still contains the two inverted site-II motifs, the putative TATA-box and the TELO-box. Similarly, the 122 bp promoter fragment, which harbors one less site-II motif compared to fragment −172, did not result in any GUS activity. Histochemical GUS staining is undetectable (Fig. 7K–O) and quantitative measurements show negligible expression levels (Fig. 8A), comparable to those found in negative control plants (pAGUS and WT). Similar construct-dependent changes of promoter activity, although less intense, were observed in floral

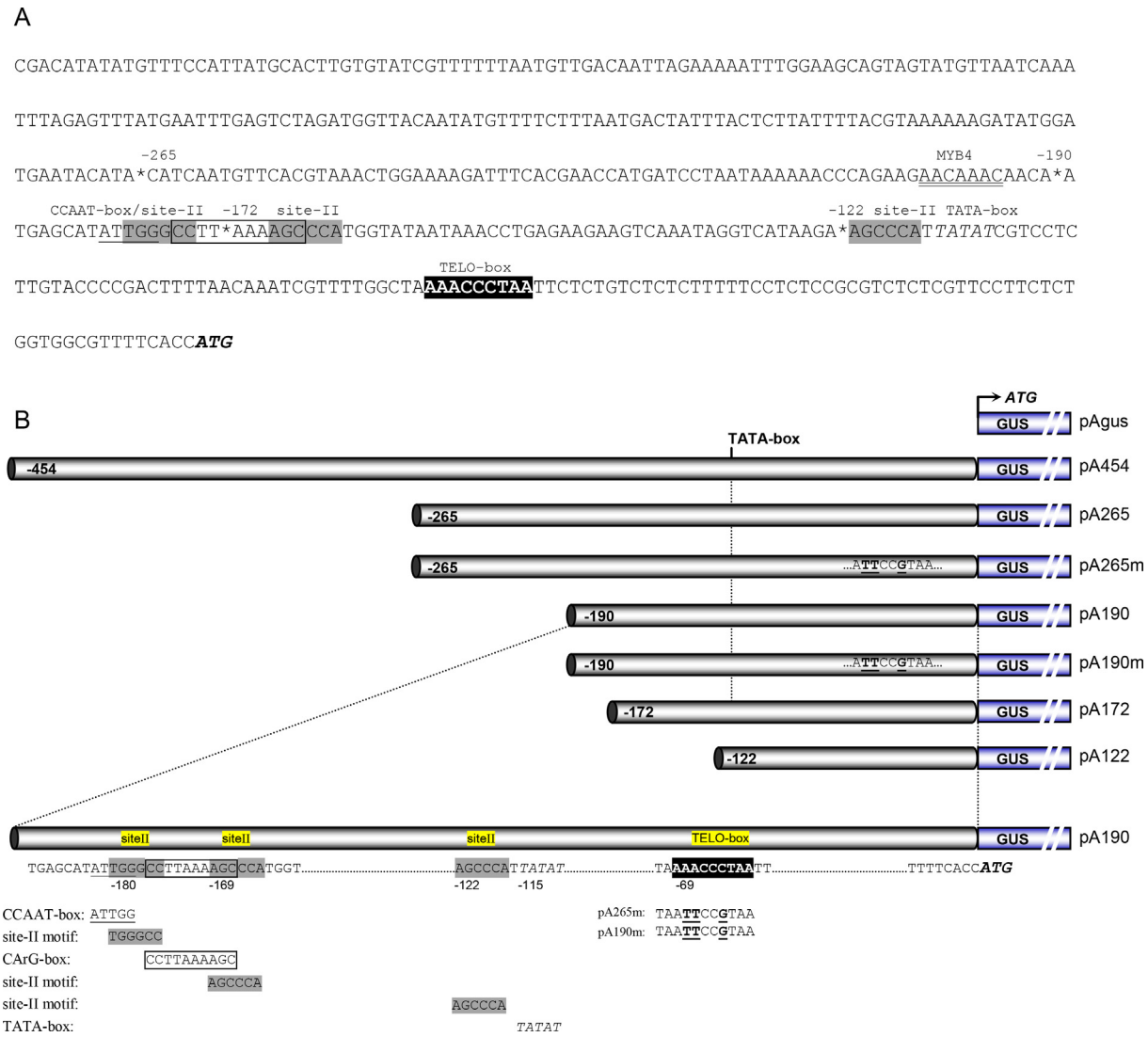


**Fig. 6.** Deletion analysis of the *AtPES* promoter. (A) Sequence analysis of the first 454 base pairs of the *AtPES* promoter. Putative *cis*-acting elements are differentially marked and labeled with their designations. The ATG start codon is shown in bold and italic letters. Asterisks and numbers above indicate the 5′ end points of the promoter fragments relative to the ATG translational start codon. (B) Schematic diagram of the successive 5′ end promoter deletion constructs fused to the GUS reporter gene. Numbers indicate base-pair positions and refer to the length of the promoter fragments relative to the ATG codon. The locations of the putative regulatory elements are shown at the bottom, while the name of each construct is given at the right side. The bold and underlined nucleotides indicate the incorporated base substitutions of the mutated TELO-box sequence in constructs pA190m and pA265m.

tissues during the reproductive developmental phase of the plants (Fig. 8B). The above results indicate that the 18 bp region within positions −190 to −172, containing the CCAAT-box, the canonical site-II motif and the CArG-box, is essential for *AtPES* expression in meristematic and rapidly dividing cells.

Since the TELO-box has been shown to play a crucial role in the expression of genes encoding ribosomal proteins and various genes expressed in cycling cells, we investigated its necessity in *AtPES* gene regulation. By employing a PCR based site-directed mutagenesis approach, we generated two additional constructs (pA265m and pA190m), in which the TELO-box sequence AAACCCTAA is mutated to ATTCCGTAA (Fig. 6B). The comparative analysis of the respective transgenic seedlings with those harboring the WT sequence revealed that mutation of the TELO-box leads to an almost complete loss of GUS activity in the root meristem, whereas only a small decrease in promoter activity is observed in the shoot meristem of the seedlings. The intensity of GUS staining is analogous in both sets of plants containing the mutated TELO-boxes and is predominantly restricted to the primordia of the developing leaves (Fig. 7D, E, I and J). In agreement with the above data, mutation of the TELO-box does not affect the GUS expression levels in open flowers, young and mature siliques. The promoter activity of constructs pA265 and pA190 is similar to that of constructs pA265m and pA190m, respectively (Fig. 8B). A small reduction in gene expression was evident only in closed flowers, which apparently harbor an increased number of meristematic cells, underlining the importance of the TELO-box binding site primarily in the root and secondarily in the shoot meristems (Figs. 7Q–T and 8B). Taken together, our results demonstrate that the TELO-box is an indispensible promoter element for the expression of the gene in root meristems, while its absence does not significantly affect *AtPES* expression in the aerial vegetative and reproductive tissues of the plants.

## 4. Discussion

The *pescadillo* orthologs from budding yeast and mammals have been shown to impinge on both ribosomal biogenesis and the cell cycle. Here we demonstrate that AtPES interacts physically

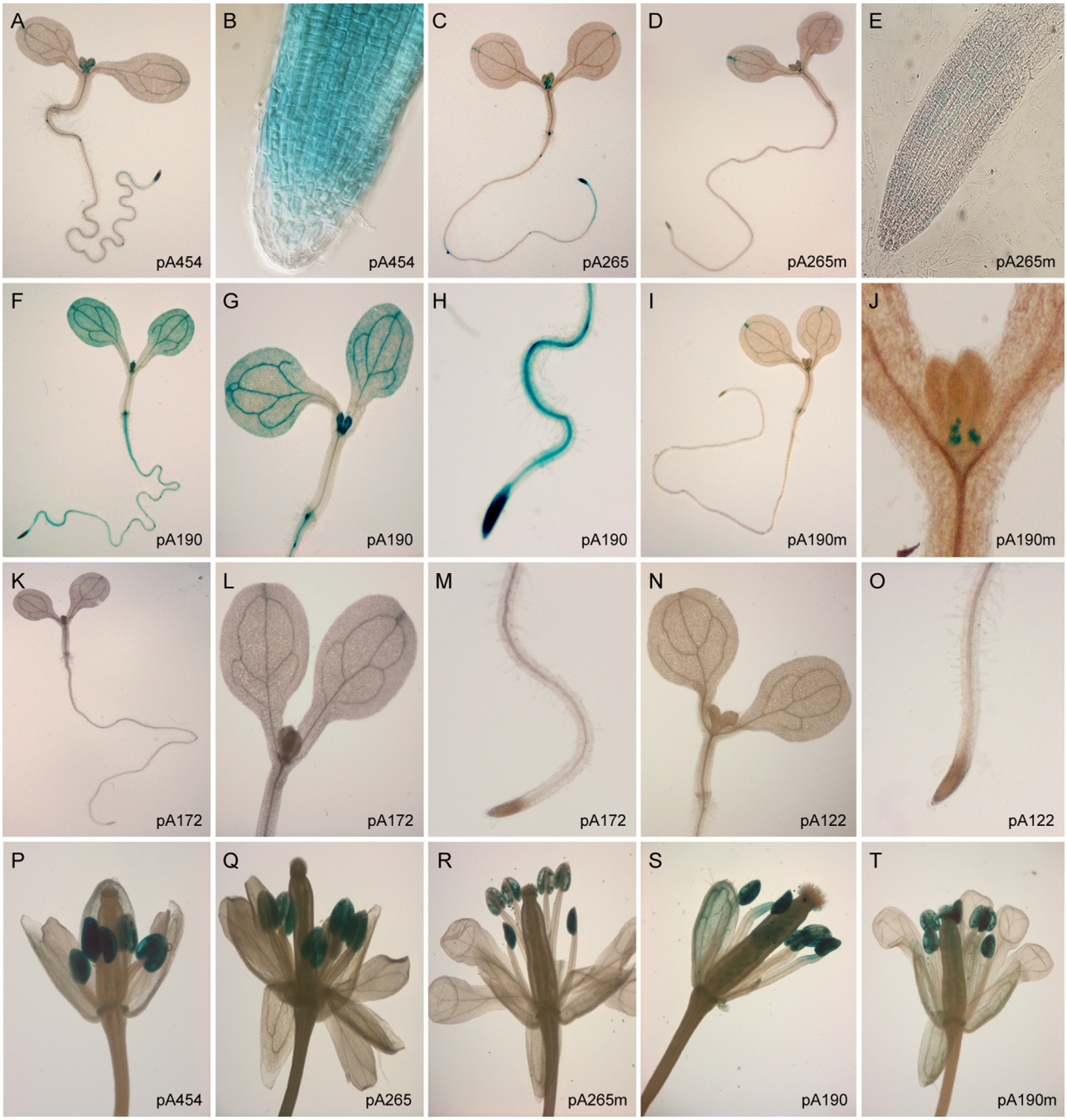


**Fig. 7.** Histochemical localization of *AtPES* promoter-GUS activity during vegetative and reproductive development. Representative GUS expression patterns in whole seedlings ((A)–(O)) and flowers ((P)–(T)) of transgenic *A. thaliana* plants harboring progressive promoter deletion constructs and the mutated TELO-box. GUS staining in both seedlings and flowers is observed with constructs containing at least 190 bp of 5′ end upstream sequences ((A)–(J) and (P)–(T)). Promoter activity is completely abolished in constructs pA172 and pA122 ((K)–(O)). Mutation of the TELO-box severely affects reporter gene expression in seedlings ((D), (E), (I) and (J)) and less in flowers ((R)–(T)).

with AtPEIP1 and AtPEIP2, the murine Bob1 and WDR12 orthologs, respectively, and that interfering with *AtPES* function *in planta* leads to a distortion of the root tip architecture. Our data are in accordance with recently published results, which also show that the depletion of the plant PES leads to morphological alteration of the nucleoli, growth arrest and acute cell death [28]. Although a compromised proliferative capacity of root TACs (transit-amplifying cells) is indicated in *AtPESi* plants, many cells in the root tip continue to grow and elongate ectopically, thus suggesting that ribosomal functions and protein synthesis might not be severely affected and that *AtPES* loss may reflect a cell cycle specific impediment. It is noteworthy that we have previously shown that the expression of the *Zinnia elegans pescadillo* ortholog (*ZePES*) is activated during G1/S transition [4]. In agreement to this hypothesis are data from yeast, showing that ribosome biogenesis is sensed independently of mature ribosome levels or protein synthetic capacity [47] and that a prerequisite for re-entering in the cell cycle is the presence of a functional Nop7 protein [9]. Moreover, the impaired function of Bop1 and/or the PeBoW complex leads to a p53-dependent cell cycle arrest in mammals [16,48,49]. In plants, depletion of PES compromises mitotic progression possibly independent of its role in ribosome biogenesis [28]. However, it is still unclear whether this compromised proliferative capacity of root TACs is directly linked to AtPES or is attributed through the plant PeBoW complex.

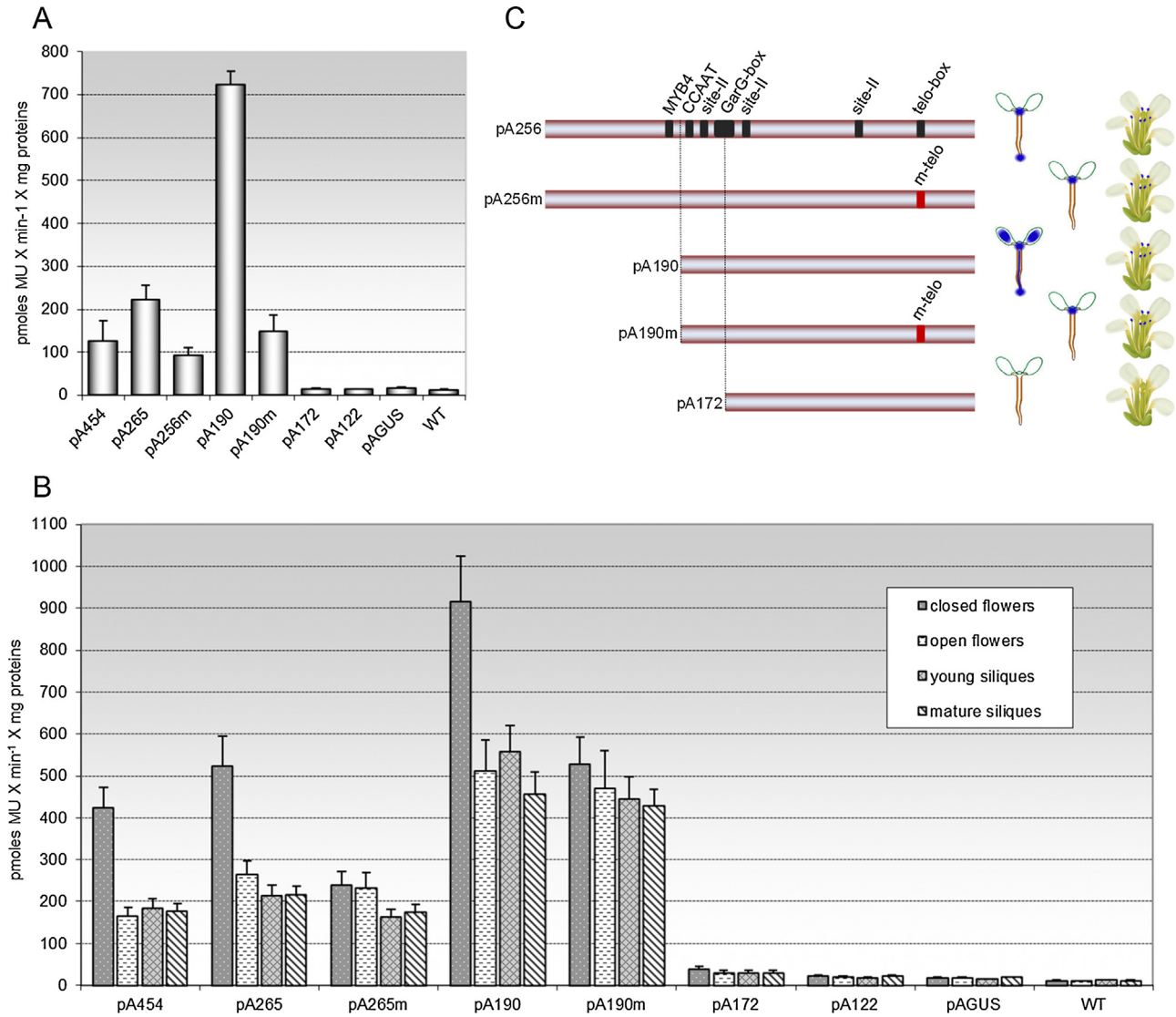


**Fig. 8.** Quantitative GUS expression analysis in entire T2 seedlings, flowers and siliques of transgenic plants harboring progressive promoter deletion constructs and the mutated TELO-box. (A) GUS activity measured in intact 7 days-old Arabidopsis seedlings. (B) Specific GUS activity in different developmental stages of floral organs. Vertical bars represent the average values of GUS fluorometric assays monitored in at least 10 independent transgenic lines. WT and pAGUS represents untransformed negative control plants and plants transformed with the promoterless GUS cassette, respectively. Error bars represent SE. (C) Schematic representation of the location of the major putative transcription factor binding sites in the *AtPES* promoter sequence and the construct-depending tissue specific GUS expression pattern in seedling and flowers.

Interfering with AtPES function hampers most likely the cell proliferation capacity in the developing root, eventually leading to the shortening of the meristematic zone. Based on our findings, however, the overall phenotype of *AtPES*–RNAi root apices is complex and points out to major, direct and/or indirect effects in the transition and elongation zones as well. The root apex of *A. thaliana* consists of three distinct zones of growth activities, namely the meristematic zone, the transition/distal elongation zone and the fast elongation zone. Each of these zones is characterized by a different tempo-spatial gene expression profile, which in turn is required for the capacity of the cells of a given zone to progress to the next one [50,51]. *AtPES* is strongly expressed in the meristematic zone, while its expression wanes in the transition zone and is undetectable in the elongation zone. Therefore, the distorted elongation zone of *AtPES*–RNAi roots may reflect indirect effects upon AtPES depletion, which have been originated in preceding zones of the root, i.e. where *AtPES* is expressed. Cells that cease division at the proximal part of the meristematic zone are unable to start elongating immediately as they must first go through a massive change in their metabolism and cytoarchitecture, events that take place in the distinct transition zone. Thus, the untimely downregulation of *AtPES* in the meristematic zone may not only inhibit cell division, but also force normal cells to enter into an abnormal, transition zone cell-like state, which in turn may limit further development. These abnormal cells exhibit an enlarged nucleus, accompanied by excessive growth and elongation. An alternative but not mutually exclusive scenario is that the highly distorted epidermal cells may impede the redistribution of auxin in the meristem and consequently the critical cascades required for proper meristem maintenance.

Promoter deletion and site-directed mutagenesis analyses clearly indicate the presence of two *cis* acting elements, namely the TELO-box and the site-II motif, as the major *cis* regulating elements for *AtPES* gene expression. TELO-boxes have been shown to act cooperatively with site-II motifs, augmenting reporter gene transcription in cycling cells. Furthermore, they co-occur in many ribosomal protein genes and genes of the general translation apparatus in Arabidopsis and rice [39,40,52]. The entire promoter exerts

a robust regulation and contributes in preserving the tissue-specific expression pattern of *AtPES*. Reporter gene expression is confined mainly in the shoot and root apices and to lesser extend in the transition zone of the root. Nevertheless, deletion of the promoter to point −190 bp results in an expansion of GUS expression not only in the shoot and root vascular tissues and the cotyledons but also in the epidermis and the root cortex, indicating the existence of suppressor elements within fragment −265 to −190. The particular fragment contains a putative R2R3 MYB4 binding site, previously implicated in transcriptional repression of genes in Arabidopsis [45,46] and may play a similar role in *AtPES* gene regulation. More importantly, this up-regulating effect is annihilated in plants transformed with the pA190m construct, harboring the mutated TELO-box, indicating that this repressor activity is TELO-box dependent. If this TELO-box/site-II mediated transcriptional repression applies also for other genes harboring this specific module, it would constitute a core significant developmental aspect in the regulation of gene expression.

Deletion of the canonical site-II motif (at position −180) results in a complete loss of promoter activity in all tissues, while mutation of the TELO-box led to a drastic reduction of *AtPES* expression specifically in root meristems, yet negligibly affecting expression in shoot meristems. In addition, disruption of the TELO-box does not have any significant impact on the expression of the reporter gene in the pollen grains of anthers. Interestingly, the fragment −190 to −172 contains overlapping sequences encompassing the canonical site-II motif, the CCAAT-box and the CArG-box. Since the CArG-box has been shown to regulate transcription of the Arabidopsis floral homeotic gene *APETALA3* [43],[44], we assume that its presence may contribute to the conservation of *AtPES* expression in pollen, independently of an existing TELO-box. Taken together, the above analysis demonstrate that a 18 bp sequence, harboring a CCAAT-box, a canonical site-II motif and a CArG-box, is indispensible for *AtPES* expression, while the TELO-box is a crucial binding site for the differential expression of the gene. However, the outstanding topic of the enzymatic counterparts of these *cis* elements remains elusive. Trémousaygue et al. [38], demonstrated that AtPura1, a plant homolog of human PUR-ALPHA (Pur-α), is capable to interact with a TELO-box in vitro. Human Pur-α binds to the hypophosphorylated form of Rb (Retinoblastoma) protein, a core cell cycle factor crucial for the G1/S transition, while in plants the homolog of RB gene (*RBR*/*RETINOBLASTOMA RELATED*) is critical for stem cell maintenance and differentiation [53]. Since a global transcriptome analysis revealed that *AtPES*, *AtPEIP1* and *AtPEIP2* are downregulated during RNAi mediated RBR silencing [54], it would be interesting to investigate the link between AtPura/TELO-box and RBR function.

However, overexpression of *AtPES* does not compromise normal plant growth and development. None of the overexpression lines exhibited any phenotypic differences compared to wild type plants under normal growth conditions. In budding yeast, pescadillo and its interactors are unstable when not incorporated in the complex, while overexpression of NOP7 does not affect growth or ribosome subunit assembly [17]. We therefore presume that *AtPES* may also be regulated at post-transcriptional levels, in order to guard the cells against any deleterious effects, which may arise from the excess of AtPES in the nucleolus.

Clearly, further research is required to elucidate the regulation of *AtPES* expression and the involvement of the corresponding protein in integral nucleolar complexes. Moreover, pescadillo has been shown to interact directly with the cadmium response element of the human heme oxygenase-1 promoter [11]. Consequently, deciphering the transcriptional regulatory networks of *AtPES* and its putative target genes may further clarify its diverse functional role in cell proliferation control and plant development.

## Conflict of interest statement

The authors declare no conflict of interest.

## Acknowledgements

The work was co-funded by the European Social Fund and National Resources (EPEAK II) PYTHAGORAS, (Grant No. 56.90.7406) and the UoA Special Account For Research Grants (S.A.R.G.), (Grant No. 70.4.7806). We thank the Salk Institute and the NASC for providing the sequence-indexed Arabidopsis T-DNA insertion lines. K.H. thanks P. Livanos for assistance with Hoechst staining and microscopy techniques and the laboratory of Prof. P. Hatzopoulos for technical assistance with the quantitative GUS measurements. The PER8 vector was kindly provided by Prof. Nam-Hai Chua. The authors also wish to apologize to those authors whose excellent work could not be cited due to space restrictions.

## Appendix A. Supplementary data

Supplementary data associated with this article can be found, in the online version, at http://dx.doi.org/10.1016/j.plantsci.2014.08.012.

## References

[1] M.L. Allende, A. Amsterdam, T. Becker, K. Kawakami, N. Gaiano, N. Hopkins, Insertional mutagenesis in zebrafish identifies two novel genes, pescadillo and dead eye, essential for embryonic development, Genes Dev. 10 (1996) 3141–3155.
[2] C.C. Adams, J. Jakovljevic, J. Roman, P. Harnpicharnchai, J.L. Woolford Jr., *Saccharomyces cerevisiae* nucleolar protein Nop7p is necessary for biogenesis of 60S ribosomal subunits, RNA 8 (2002) 150–165.
[3] J. Haque, S. Boger, J. Li, S.A. Duncan, The murine Pes1 gene encodes a nuclear protein containing a BRCT domain, Genomics 70 (2000) 201–210.
[4] A. Zografidis, G. Kapolas, G. Kitsios, M. McCann, K. Roberts, D. Milioni, K. Haralampidis, Isolation and characterization of *ZePES* and *AtPES*, the pescadillo orthologs from Zinnia and Arabidopsis, Plant Sci. 173 (2007) 358–369.
[5] X. Yu, C.C. Chini, M. He, G. Mer, J. Chen, The BRCT domain is a phospho-protein binding domain, Science 302 (2003) 639–642.
[6] M. Hölzel, M.T. Grimm, M. Rohrmoser, A. Malamoussi, T. Harasim, A. Gruber-Eber, E. Kremmer, D. Eick, The BRCT domain of mammalian Pes1 is crucial for nucleolar localization and rRNA processing, Nucleic Acids Res. 35 (2007) 789–800.
[7] A. Lerch-Gaggl, J. Haque, J. Li, G. Ning, P. Traktman, S.A. Duncan, Pescadillo is essential for nucleolar assembly, ribosome biogenesis, and mammalian cell proliferation, J. Biol. Chem. 277 (2002) 45347–45355.
[8] M. Oeffinger, A. Leung, A. Lamond, D. Tollervey, Yeast Pescadillo is required for multiple activities during 60S ribosomal subunit synthesis, RNA 8 (2002) 626–636.
[9] Y.C. Du, B. Stillman, Yph1p, an ORC-interacting protein: potential links between cell proliferation control, DNA replication, and ribosome biogenesis, Cell 109 (2002) 835–848.
[10] A. Killian, N. Le Meur, R. Sesboue, J. Bourguignon, G. Bougeard, J. Gautherot, C. Bastard, T. Frebourg, J.M. Flaman, Inactivation of the RRB1-Pescadillo pathway involved in ribosome biogenesis induces chromosomal instability, Oncogene 23 (2004) 8597–8602.
[11] E.M. Sikorski, T. Uo, R.S. Morrison, A. Agarwal, Pescadillo interacts with the cadmium response element of the human heme oxygenase-1 promoter in renal epithelial cells, J. Biol. Chem. 28 (2006) 24423–24430.
[12] A.F. Lerch-Gaggl, K. Sun, S.A. Duncan, Light chain 1 of microtubule-associated protein 1B can negatively regulate the action of Pes1, J. Biol. Chem. 282 (2007) 11308–11316.
[13] A. Fatica, D. Tollervey, Making ribosomes, Curr. Opin. Cell Biol. 14 (2002) 313–318.
[14] S. Granneman, S.J. Baserga, Ribosome biogenesis: of knobs and RNA processing, Exp. Cell Res. 296 (2004) 43–50.
[15] T. Pederson, R.Y. Tsai, In search of nonribosomal nucleolar protein function and regulation, J. Cell Biol. 184 (2009) 771–776.
[16] M. Hölzel, M. Rohrmoser, M. Schlee, T. Grimm, T. Harasim, A. Malamoussi, A. Gruber-Eber, E. Kremmer, W. Hiddemann, G.W. Bornkamm, D. Eick, Mammalian WDR12 is a novel member of the Pes1–Bop1 complex and is required for ribosome biogenesis and cell proliferation, J. Cell Biol. 170 (2005) 367–378.
[17] L. Tang, A. Sahasranaman, J. Jakovljevic, E. Schleifman, J.L. Woolford Jr., Interactions among Ytm1, Erb1, and Nop7 required for assembly of the Nop7-subcomplex in yeast preribosomes, Mol. Biol. Cell 19 (2008) 2844–2856.

[18] Y.R. Lapik, C.J. Fernandes, L.F. Lau, D.G. Pestov, Physical and functional interaction between Pes1 and Bob1 in mammalian ribosome biogenesis, Mol. Cell 15 (2004) 17–29.
[19] Z. Strezoska, D.G. Pestov, L.F. Lau, Bop1 is a mouse WD40 repeat nucleolar protein involved in 28S and 5.8S RRNA processing and 60S ribosome biogenesis, Mol. Cell Biol. 20 (2000) 5516–5528.
[20] M. Rohrmoser, M. Hölzel, T. Grimm, A. Malamoussi, T. Harasim, M. Orban, I. Pfisterer, A. Gruber-Eber, E. Kremmer, D. Eick, Interdependence of Pes1, Bop1, and WDR12 controls nucleolar localization and assembly of the PeBoW complex required for maturation of the 60S ribosomal subunit, Mol. Cell Biol. 27 (2007) 3682–3694.
[21] D.G. Pestov, M.G. Stockelman, Z. Strezoska, L.F. Lau, ERB1, the yeast homolog of mammalian Bop1, is an essential gene required for maturation of the 25S and 5.8S ribosomal RNAs, Nucleic Acids Res. 29 (2001) 3621–3630.
[22] P. Shaw, J. Doonan, The nucleolus: playing by different rules? Cell Cycle 4 (2005) 102–105.
[23] E. Ramirez-Parra, B. Desvoyes, C. Gutierrez, Balance between cell division and differentiation during plant development, Int. J. Dev. Biol. 49 (2005) 467–477.
[24] C. Gutierrez, Coordination of cell division and differentiation, in: D.P.S. Verma, Z. Hong (Eds.), Plant Cell Monographs 9, Springer-Verlag, Berlin Heidelberg, 2008, pp. 377–393.
[25] X. Zhao, H. Harashima, N. Dissmeyer, S. Pusch, A.K. Weimer, J. Bramsiepe, D. Bouyer, S. Rademacher, M.K. Nowack, B. Novak, S. Sprunck, A. Schnittger, A general G1/S-phase cell-cycle control module in the flowering plant *Arabidopsis thaliana*, PLoS Genet. 8 (2012) e1002847.
[26] B.M. Horváth, Z. Magyar, Y. Zhang, A.W. Hamburger, L. Bakó, R.G. Visser, C.W. Bachem, L. Bögre, EBP1 regulates organ size through cell growth and proliferation in plants, EMBO J. 25 (2006) 4909–4920.
[27] P.C.K. Huang, L.F. Huang, J.J. Huang, S.J. Wu, C.H. Yeh, C.A. Lu, A DEAD-box protein, AtRH36, is essential for female gametophyte development and is involved in rRNA biogenesis in Arabidopsis, Plant Cell Physiol. 51 (2010) 694–706.
[28] H.K. Cho, C.S. Ahn, H.S. Lee, J.K. Kin, H.S. Pai, Pescadillo plays an essential role in plant cell growth and survival by modulating ribosome biogenesis, Plant J. 76 (2013) 393–405.
[29] J. Zuo, Q.W. Niu, N.H. Chau, An estrogen receptor-based transactivator XVE mediates highly inducible gene expression in plants, Plant J. 24 (2000) 265–273.
[30] G. An, P.R. Edbert, A. Mitra, S.B. Ha, Binary vectors, in: S.B. Gelvin, R.A. Shilperoort, D.P.S. Verma (Eds.), Plant Molecular Biology Manual, Kluwer Academic Publishers, Dordrecht, 1988, pp. 1–9.
[31] N. Bechtold, G. Pelletier, *In planta* Agrobacterium-mediated transformation of adult *Arabidopsis thaliana* plants by vacuum infiltration, Methods Mol. Biol. 82 (1998) 259–266.
[32] O. Voinnet, S. Rivas, P. Mestre, D. Baulcombe, An enhanced transient expression system in plants based on suppression of gene silencing by the p19 protein of tomato bushy stunt virus, Plant J. 33 (2003) 949–956.
[33] M. Walter, C. Chaban, K. Schütze, O. Batistic, K. Weckermann, C. Näke, D. Blazevic, C. Grefen, K. Schumacher, C. Oecking, K. Harter, J. Kudla, Visualization of protein interactions in living plant cells using bimolecular fluorescence complementation, Plant J. 40 (2004) 428–438.
[34] T. Ishida, S. Fujiwara, K. Miura, N. Stacey, M. Yoshimura, K. Schneider, S. Adachi, K. Minamisawa, M. Umeda, K. Sugimoto, SUMO E3 ligase HIGH PLOIDY2 regulates endocycle onset and meristem maintenance in Arabidopsis, Plant Cell 21 (2009) 2284–2297.
[35] P. Shaw, The Nucleolus, Nature Encyclopedia of Life Sciences 4, Nature Publishing Group, 2001, E0395802.
[36] P. Shaw, J. Brown, Plant nuclear bodies, Curr. Opin. Plant Biol. 7 (2004) 614–620.
[37] S. van Nocker, P. Ludwig, The WD-repeat protein superfamily in Arabidopsis: conservation and divergence in structure and function, BMC Genomics 4 (2003) 50.
[38] D. Trémousaygue, A. Manevski, C. Bardet, N. Lescure, B. Lescure, Plant interstitial telomere motifs participate in the control of gene expression in root meristems, Plant J. 20 (1999) 553–561.
[39] A. Manevski, G. Bertoni, C. Bardet, D. Tremousaygue, B. Lescure, In synergy with various *cis*-acting elements, plant insterstitial telomere motifs regulate gene expression in *Arabidopsis* root meristems, FEBS Lett. 483 (2000) 43–46.
[40] D. Trémousaygue, L. Garnier, C. Bardet, P. Dabos, C. Hervé, B. Lescure, Internal telomeric repeats and 'TCP domain' protein-binding sites co-operate to regulate gene expression in *Arabidopsis thaliana* cycling cells, Plant J. 33 (2003) 957–966.
[41] T. Miwa, L. Kedes, Duplicated CArG box domains have positive and mutually dependent regulatory roles in expression of the human a-cardiac actin gene, Mol. Cell Biol. 7 (1987) 2803–2813.
[42] N.A. Kane, Z. Agharbaoui, A.O. Diallo, H. Adam, Y. Tominaga, F. Ouellet, F. Sarhan, TaVRT2 represses transcription of the wheat vernalization gene TaVRN1, Plant J. 51 (2007) 670–680.
[43] J.J. Tilly, D.W. Allen, T. Jack, The CArG boxes in the promoter of the Arabidopsis floral organ identity gene APETALA3 mediate diverse regulatory effects, Development 125 (1998) 1647–1657.
[44] T.A. Hill, C.D. Day, S.C. Zondlo, A.G. Thackeray, V.F. Irish, Discrete spatial and temporal *cis*-acting elements regulate transcription of the Arabidopsis floral homeotic gene APETALA3, Development 125 (1998) 1711–1721.
[45] H. Jin, E. Cominelli, P. Bailey, A. Parr, F. Mehrtens, J. Jones, C. Tonelli, B. Weisshaar, C. Martin, Transcriptional repression by AtMYB4 controls production of UV-protecting sunscreens in Arabidopsis, EMBO J. 19 (2000) 6150–6161.
[46] J. Zhao, W. Zhang, Y. Zhao, X. Gong, L. Guo, G. Zhu, X. Wang, Z. Gong, K.S. Schumaker, Y. Guo, SAD2, an importin-like protein, is required for UV-B response in Arabidopsis by mediating MYB4 nuclear trafficking, Plant Cell 19 (2007) 3805–3818.
[47] K.A. Bernstein, F. Bleichert, J.M. Bean, F.R. Cross, S.J. Baserga, Ribosome biogenesis is sensed at the Start cell cycle checkpoint, Mol. Biol. Cell 18 (2007) 953–964.
[48] D.G. Pestov, Z. Strezoska, L.F. Lau, Evidence of p53-dependent cross-talk between ribosome biogenesis and the cell cycle: effects of nucleolar protein Bop1 on G(1)/S transition, Mol. Cell Biol. 21 (2001) 4246–4255.
[49] T. Grimm, M. Hölzel, M. Rohrmoser, T. Harasim, A. Malamoussi, A. Gruber-Eber, E. Kremmer, D. Eick, Dominant-negative Pes1 mutants inhibit ribosomal RNA processing and cell proliferation via incorporation into the PeBoW-complex, Nucleic Acids Res. 34 (2006) 3030–3043.
[50] J.P. Verbelen, T. De Cnodder, J. Le, K. Vissenberg, F. Baluška, The root apex of *Arabidopsis thaliana* consists of four distinct zones of cellular activities: meristematic zone, transition zone, fast elongation zone, and growth terminating zone, Plant Signal. Behav. 1 (2006) 296–304.
[51] P. Derbyshire, S. Drea, P.J. Shaw, J.H. Doonan, L. Dolan, Proximal-distal patterns of transcription factor gene expression during Arabidopsis root development, J. Exp. Bot. 59 (2008) 235–245.
[52] C. Gaspin, J.F. Rami, B. Lescure, Distribution of short interstitial telomere motifs in two plant genomes: putative origin and function, BMC Plant Biol. 10 (2010) 283.
[53] M. Wildwater, A. Campilho, J.M. Perez-Perez, R. Heidstra, I. Blilou, H. Korthout, J. Chatterjee, L. Mariconti, W. Gruissem, B. Scheres, The RETINOBLASTOMA-RELATED gene regulates stem cell maintenance in Arabidopsis roots, Cell 123 (2005) 1337–1349.
[54] L. Borghi, R. Gutzat, J. Fütterer, Y. Laizet, L. Hennig, W. Gruissem, Arabidopsis RETINOBLASTOMA-RELATED is required for stem cell maintenance, cell differentiation, and lateral organ production, Plant Cell 22 (2010) 1792–1811.